Diffuse Whistler Mode Waves Detected by Kaguya in Lunar Polar Region

T. Nakagawa[1], F. Takahashi[2], H. Shimizu[3], and Y. Saito[4]

[1]Department of Information and Communication Engineering, Tohoku Institute of Technology, Miyagi, 982-8577 Japan.

[2]Department of Earth and Planetary Sciences, Faculty of Science, Kyushu University, Fukuoka 819-0395.

[3]Earthquake Research Institute, University of Tokyo, Tokyo 113-0032, Japan.

[4]Institute of Space and Astronautical Science, Japan Aerospace Exploration Agency, Kanagawa, 229-8510 Japan.

Corresponding author: Tomoko Nakagawa (nakagawa@tohtech.ac.jp)

Key Points:

- Diffuse emission of whistler mode waves from 1 to 16 Hz were found over the polar regions of the moon in the solar wind.
- They were right-handed, parallel-propagating waves with respect to the background magnetic field, without significant Doppler-shift.
- They are thought to be generated by solar wind ions reflected by the moon and propagate along field lines convected by the solar wind.

Abstract

Solar wind particles reflected by the lunar magnetic field are major energy source of electromagnetic wave activities around the moon. In addition to known waves such as 100 s magnetohydrodynamic waves and 1 Hz whistler mode waves generated by protons, or non-monochromatic whistler mode waves generated by mirror-reflected electron beams, Kaguya found a new type of whistler mode waves at an altitude of 100 km above the polar regions of the moon, not above intense magnetic anomalies. The frequency range 1-16 Hz was broad like the non-monochromatic waves generated by electron beams, but their occurrence was less sensitive to the magnetic connection like the waves generated by reflected protons. They appear diffuse both in time and frequency domains, and the polarization was right-handed with respect to the background magnetic field. The wave number vector was nearly parallel to the background magnetic field which was perpendicular to the solar wind flow. The diffuse waves are thought to be generated by solar wind ions reflected by the lunar magnetic field through cyclotron resonance. The resonant ions were expected to have velocity component parallel to the magnetic field larger than the solar wind bulk speed, but such ions were not always detected simultaneously. There is a possibility that the waves were generated above the dayside moon and then propagated along the magnetic field convected by the solar wind to reach polar regions to be detected by Kaguya.

Plain Language Summary

As the moon is not shielded by global magnetic field like the Earth, the solar wind particles can access the lunar surface. Although most of them are absorbed by the surface, a small fraction is scattered by the surface or reflected by intense lunar magnetic fields (so called magnetic anomalies) back into the solar wind and become an energy source of wave activities. Protons reflected by the magnetic anomalies are responsible for generation of 0.01 Hz ultra-low frequency waves or 1 Hz electron cyclotron waves. Electrons reflected by the lunar magnetic field form a field aligned beam responsible for generation of non-monochromatic electromagnetic waves whose detection is controlled by the magnetic connection. Kaguya found a new type of electromagnetic waves with broad frequency range like the non-monochromatic waves generated by electrons, but less sensitive to the magnetic connection like the waves generated by reflected protons. They were preferentially observed above the polar region of the moon, not above intense magnetic anomalies. They were thought to be generated by solar wind ions reflected by the lunar magnetic fields and propagate along the solar wind magnetic field to the polar region being convected down the solar wind flow.

1 Introduction

Due to the lack of global scale magnetic field or dense atmosphere, the solar wind particles hit the moon directly and most of them are absorbed by the surface, leaving a plasma void called a lunar wake on the downstream side (Lyon et al., 1967; Colburn et al., 1967; Schubert & Lichtenstein, 1974; Bosqued et al. 1996; Ogilvie et al. 1996). On the other hand, a small fraction of them have been found to be scattered, reflected, or diffracts by the lunar surface or its crustal magnetic field. Observations from Kaguya and Chandrayaan-1 have revealed that a small fraction (0.1 – 1%) of the incident plasmas was found to be backscattered by the lunar surface, while 10 – 50% were reflected by the local crustal field, called magnetic anomaly (Saito et al., 2008, 2010; Lue et al., 2011). Above the magnetic anomalies, deceleration of ions and acceleration of electrons parallel to the magnetic field, together with heating of reflected ions were observed (Saito et al., 2012). Chandrayaan-1 and IBEX have shown up to 20% of the incident solar wind particles were backscattered in the form of energetic neutral hydrogen atoms with energy of several tens of eV, and some of them experience charge exchange with the ambient plasma to behave as reflected protons thereafter (McComas et al., 2009; Wieser et al., 2009, 2011; Poppe et al., 2014; Bhardwaj et al., 2015).

The backscattered, reflected or diffracted particles are main source of the various wave activities (e.g., Harada et al., 2015; Nakagawa, 2016; Harada & Halekas, 2016, and references therein). In this paper, we concentrate low frequency waves. Among them, most prominent are 0.01 Hz ultra-low frequency (ULF) waves (Nakagawa et al., 2012) and 1 Hz whistler mode waves generated by reflected protons (Halekas et al., 2006b; Tsugawa et al., 2011), and non-monochromatic whistler mode waves in the extremely low frequency (ELF) range generated by reflected electrons (Nakagawa et al., 2011). Figure 1 shows typical examples.

The ULF and whistler mode waves generated by protons were characterized by narrow bandwidth and occurrence property less sensitive to the magnetic connection between the observer and the lunar surface, due to the large gyro radius of the protons. Red and blue bars at the bottom of each spectrum in Figure 1 indicate that linearly extrapolated line of force of the magnetic field at the spacecraft intersects dayside or nightside surface of the moon, respectively. The waves were continuously observed while the magnetic connection was intermittent, and the appearance or disappearance were not controlled by the magnetic connection.

They were generated by ions reflected into the direction nearly antiparallel to the solar wind flow through cyclotron resonant interaction with solar wind magnetohydrodynamic (MHD) waves or whistler mode waves, and the Doppler-shifted and detected as narrow-band waves often with left-handed polarization with respect to the background magnetic field.

On the other hand, mirror-reflected electrons above the lunar crustal magnetic field generate non-monochromatic whistler mode waves over a frequency range from 0.1 to 10 Hz (Nakagawa et al., 2011; Tsugawa et al., 2012). Their occurrence was severely controlled by magnetic connection of spacecraft to the lunar surface, suggesting that the energy source was particles bound to the magnetic field lines within a small gyroradius. The wave intensity was high when the spacecraft was magnetically connected to the magnetic anomaly, while the wave activity was depressed as soon as the magnetic field was disconnected from the lunar surface.

In addition to these known waves, a new type of diffuse ELF waves was found by Kaguya above the polar region of the moon. They are diffuse emission in a broad frequency range from 1 to 16 Hz like ELF waves generated by electrons, while their occurrence was not sensitive to the background magnetic field like the whistler mode waves generated by protons. This paper reports the property and the generation mechanism.

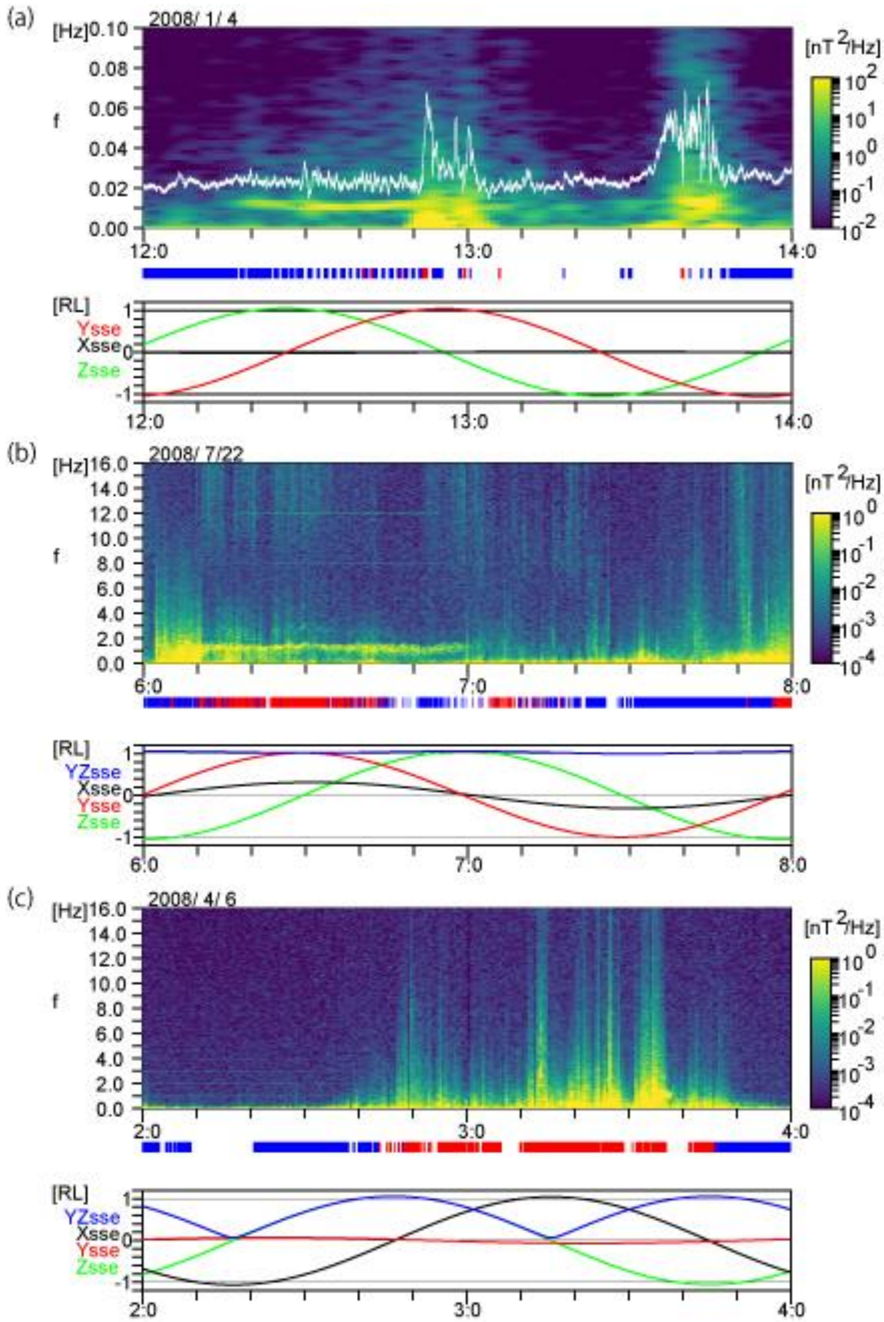

Figure 1. Examples of low-frequency waves detected by Kaguya at an altitude of 100 km above the lunar surface. (a) Ultra-low frequency (ULF) waves at 0.010-0.012 Hz and (b) whistler mode waves at 1.1 – 1.4 Hz generated by reflected ions, and (c) non-monochromatic extremely-low

frequency (ELF) waves generated by reflected electrons. Red (blue) bars at the bottom of each spectrum indicate that linearly extrapolated line of force of the magnetic field at the spacecraft intersects dayside (nightside) surface of the moon, respectively.

2 Data

Magnetic field and plasma data used in this study were obtained by Lunar MAGnetometer (LMAG) and Plasma energy Angle and Composition Experiment (PACE) of the MAgnetic field and Plasma experiment (MAP) (Saito et al., 2008, 2010; Tsunakawa et al., 2010; Shimizu et al., 2008) onboard Kaguya on its polar orbit around the moon during the period from January 1, 2008 to September 30, 2008. The altitude of the spacecraft was about 100 km above the lunar surface (Kato et al., 2010). The period of orbital motion was approximately 2 hours.

Magnetic field vectors obtained by LMAG at a sampling frequency of 32 Hz (Takahashi et al., 2009) were Fourier transformed every 32 sec. Minimum variance analysis (Sonnerup and Cahill, 1967) was applied to each Fourier component to obtain direction of wavenumber vector **k**. The **k** vector was assumed to be parallel to the minimum direction. The intermediate and maximum variance components were separated into left-hand or right-hand polarized components with respect to the background magnetic field. The sense of rotation (polarization) with respect to the background magnetic field of the wave was defined as $(B_L^2 - B_R^2)/(B_L^2 + B_R^2)$, where B_L and B_R are amplitudes of the left-handed or right-handed components, respectively.

Three-dimensional energy distribution of ions and electrons were obtained by 4 sensors of MAP-PACE, IEA (Ion Energy Analyzed), IMA (Ion Mass Analyzed) for ions and ESA (Electron Spectrum Analyzed)-S1 and ESA-S2 for electrons. The IMA and ESA-1 sensors were installed on the nadir-looking panel of the spacecraft to detect particles coming from the moon, while the IEA and ESA-2 sensors were on the zenith-looking panel (Saito et al., 2010).

Upstream solar wind condition was monitored by using Level 2 data from the Solar Wind Electron, Proton, and Alpha Monitor (SWEPAM) onboard the Advanced Composition Explorer (ACE) spacecraft. The data were extracted from NASA/GSFC's OMNI data set through OMNIWeb Plus.

3 Observations

3.1 Diffuse ELF waves in the solar wind

Figure 2 shows an example of diffuse ELF waves found by Kaguya on March 8, 2008, when the moon was in the solar wind (Figure 3a). A diffuse emission was observed in a frequency range from 4 Hz to 16 Hz during the period from 7:03 to 7:13 when the spacecraft was above the southern polar region of the moon (Figure 2f and Figures 3c-3d). In the previous evolution of the spacecraft, faint, but similar waves were seen from 5:11 to 5:17 in a range 6-12 Hz over the same southern polar region. The frequency range was between ion- and electron cyclotron frequencies 0.075 Hz and 0.14 kHz (for the magnetic field 4.9 nT at 7:05), close to the lower hybrid frequency 3.2 Hz (calculated from with plasma density 8.0×10^6 m^{-3}). Figure 4 compares a cross-cut spectrum of power density of the diffuse wave (Figure 4b) with that for a quiet period (Figure 4a). The power density enhanced over a wide range from 4 Hz to 16 Hz.

The diffuse waves were detected on field lines disconnected from the moon. The blanks in Figure 2b indicate that Kaguya was magnetically disconnected from the lunar surface. The background magnetic field $\mathbf{B}_0$ was almost in y_{sse} direction of the selenocentric solar ecliptic (sse) coordinate system during the detection of the diffuse ELF waves (Figure 2g).

Figure 2c shows the sense of polarization in spacecraft frame of reference for each Fourier component whose power density was greater than 5×10^{-3} nT^2/Hz. Red color indicates right-hand polarizations with respect to the background magnetic field. The polarization of the diffuse ELF waves was predominantly right-handed with respect to the background magnetic field.

The wave number vector **k** of the diffuse ELF was nearly parallel to the background magnetic field $\mathbf{B}_0$. Figure 2d shows the angle $\theta_{\mathbf{k}\cdot\mathbf{B}_0}$ between the vectors **k** and $\mathbf{B}_0$. Red color indicates that the vector **k** was parallel to $\mathbf{B}_0$. The polarization and the propagation direction suggest that the diffuse ELF emissions were whistler mode waves. No significant Doppler shift was expected because the **k** vector was nearly perpendicular to the bulk flow of the solar wind in x_{sse} direction (Figure 2e).

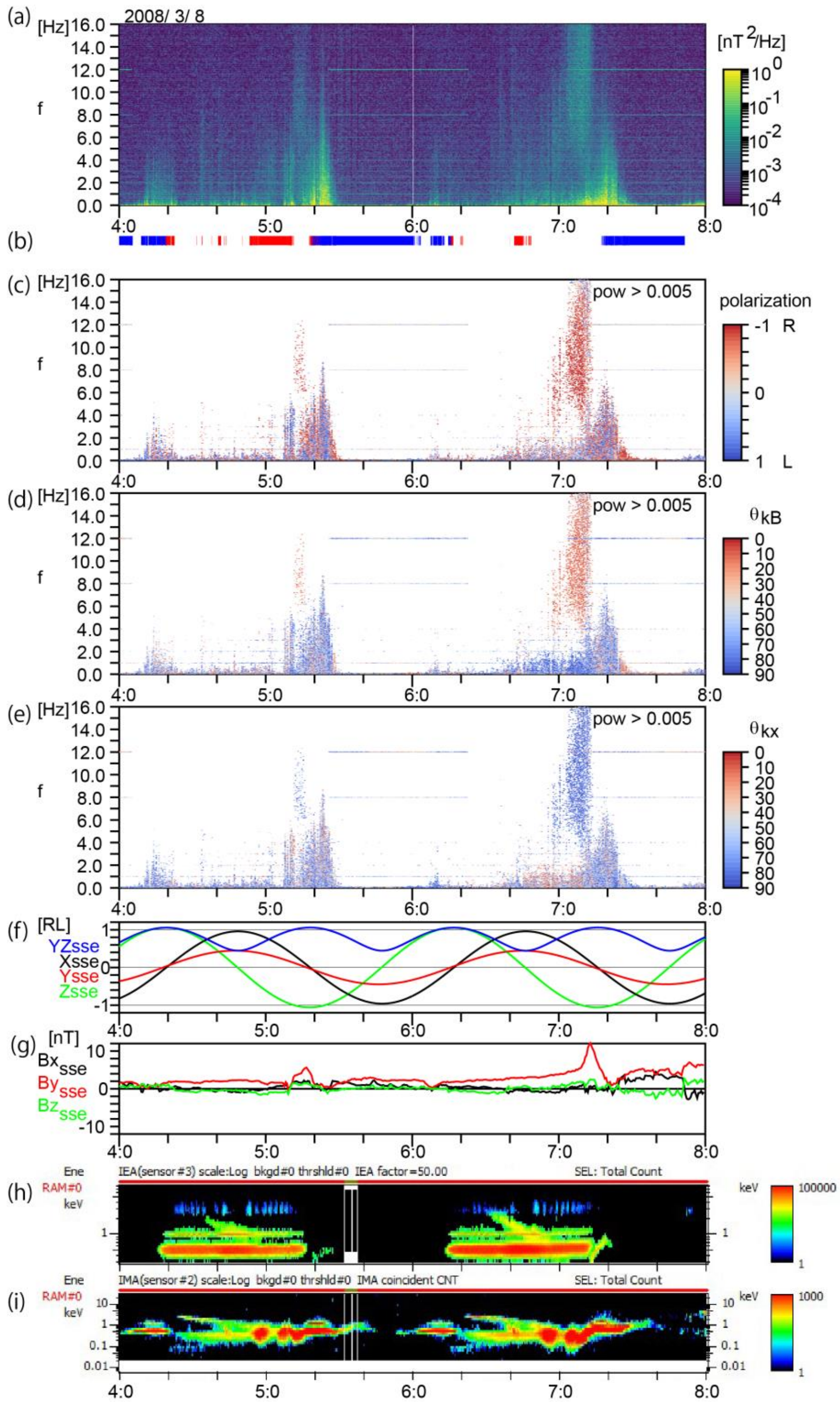

Figure 2. A diffuse ELF event observed by Kaguya at an altitude of 100 km above the moon on March 8, 2008. (a) Power density of magnetic fluctuation, (b) magnetic connection of Kaguya to the nightside (blue) or dayside (red) surface of the moon, estimated by linearly extrapolated line of force of the magnetic field at Kaguya, (c) sense of rotation of the magnetic field variation with respect to the background magnetic field (red for right-hand and blue for left-hand), (d) the angle

between **k** vector and the background magnetic field $\mathbf{B}_0$ for the Fourier components whose power density was larger than $0.005\,\mathrm{nT}^2/\mathrm{Hz}$, (e) the angle between **k** vector and the x_{sse} axis of the selenocentric solar ecliptic (sse) coordinate system, (f) position of Kaguya ($x_{sse}, y_{sse}, z_{sse}$) together with the distance $\sqrt{y_{sse}^2 + z_{sse}^2}$ from the x_{sse} axis, (g) 32s-averaged background magnetic field, (h) omni-directional energy-time spectrogram of ions from IEA sensor of PACE looking zenith direction and (i) from IMA sensor facing the lunar surface.

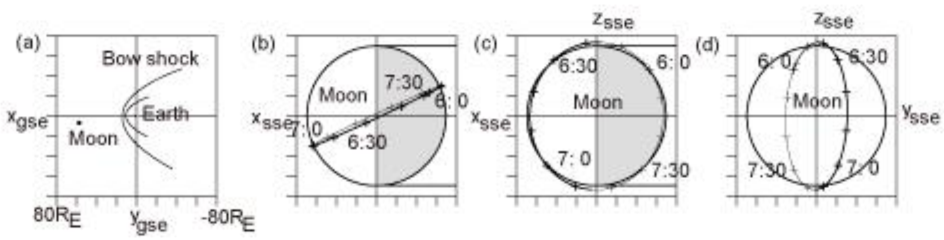

Figure 3. Position of Kaguya at the detection of the diffuse ELF waves on March 8, 2008. (a) Position of the moon in geocentric solar ecliptic (gse) coordinates. (b)(c)(d) Kaguya position projected on (b) x-y, (c) x-z, and (d) y-z planes of the selenocentric solar ecliptic (sse) coordinate system.

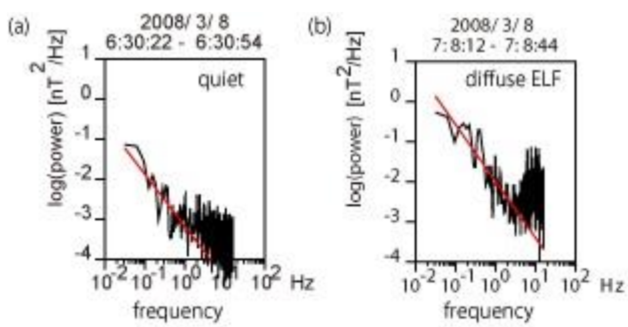

Figure 4. Spectra of magnetic field variation observed by Kaguya around the moon on March 8, 2008. (a) A quiet period from 6:30:22 to 6:30:54 and (b) a diffuse ELF wave period from 7:08:12 to 7:08:44. Black curves are power density calculated by Fourier transform of 32 Hz magnetic field data applied for every 32 s. Red lines are linear fit to the observed spectra in a low frequency range from 0.031 Hz to 1 Hz. The power density of higher frequency range in panel (a) gives a measure of noise level. Enhancements in panel (b) over a frequency range from 4 to 16 Hz were significantly higher than the noise level.

The diffuse waves were not detected above intense magnetic anomalies. Figure 5 shows Kaguya position during the detection of the diffuse wave. Color coded is the magnitude of the crustal magnetic field at the lunar surface calculated from Kaguya observation (Tsunakawa et al., 2015). There was no intense magnetic field at Kaguya position, while most intense magnetic anomalies on the moon extended sunward and equatorward of Kaguya on this day.

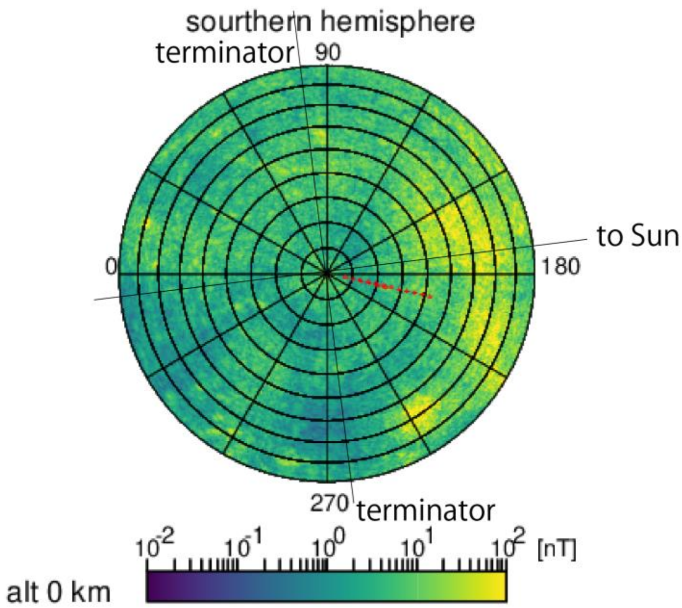

Figure 5. Kaguya position during diffuse ELF waves and the lunar crustal magnetic field. Colors indicate magnitude of the magnetic field at an altitude of 0 km (Tsunakawa et al., 2015) on the Lambert azimuthal equal area projection. Kaguya position (red crosses) was plotted every 1 minute from 5:11 to 5:17 and from 7:03 to 7:13 on March 8, 2008.

Figure 2g shows that the diffuse ELF waves were observed on the positive gradient of the magnitude toward a Lunar External Magnetic enhancement (LEME, see Halekas et al., 2006a) with peak magnitude at 7:13. It was also recognized at 5:17. The diffuse waves disappeared at the peak of the LEME. Another type of low frequency wave was observed at the LEME, but their properties of mixed polarization and direction of wave number vectors were quite different from the diffuse ELF waves.

Figures 2h and 2i show energy spectra of the ions detected by IEA and IMA sensors of MAP-PACE, respectively. During the detection of the diffuse ELF wave, IMA observed a bunch of protons reflected by a crustal field from 7:02 to 7:10 in the energy range from 0.1 to 1 keV, but the start and end times of the reflected ions were not exactly the same as that of the diffuse ELF waves. IEA detected incident solar wind ions centered at 0.5 keV consistently with ACE observation of 330 km/s at 1.52×10^{6} km upstream in the solar wind shifted by about 1 hour for traveling the distance. The upstream number density of the solar wind at ACE was $2\times10^{7}\ \mathrm{m}^{-3}$, which was higher than nominal value of the solar wind.

IMA detected another bunch of reflected protons from 6:53 to 7:00, but they were not accompanied by diffuse ELF waves.

3.2 Diffuse ELF waves in the magnetosheath

Figure 6 shows another diffuse ELF event found in the Earth's magnetosheath. Kaguya was on the nightside of the terminator but was exposed to the magnetosheath flow (Figure 7c-d ad Figure 8). A diffuse emission was found in a frequency range from 1 Hz to 8 Hz during the period from 20:40 to 21:00 on June 14, 2008 above the northern polar region of the moon. The emission appeared diffuse both in time and frequency domains. It makes a clear contrast with broadband emissions with sharp appearance and mixed polarization observed from 21:00 to 22:00.

The observed frequency 1 – 8 Hz corresponds to 3 – 27 times the ion cyclotron frequency 0.3 Hz calculated from the magnitude of the background magnetic field 19.4 – 22.1 nT. Three lanes of falling tone starting at around 20:40, 20:45 and 20:50 were recognized in Figure 6. The polarization was again right-handed with respect to the background magnetic field, and the **k** vector was again nearly parallel to the magnetic field. Because the magnetic field was almost in southward direction (Figure 6g) the **k** vector was nearly perpendicular to the bulk flow of the magnetosheath plasma (Figure 6e), an effect of Doppler shift was supposed to be small.

Throughout the diffuse ELF wave event, Kaguya was magnetically connected to the lunar surface as recognized from Figure 6b. Figures 8 and 9 show that there was no intense crustal magnetic field at the foot of the magnetic field line.

The diffuse appearance and insensitiveness to the magnetic connection suggest that the emission was generated by ions. An attempt was made to search ions that would generate the waves in PACE observation in Figures 6h and 6i, but it was difficult to distinguish reflected ions from the incident solar wind component because the latter also entered IMA sensor of Kaguya on this orbit just behind the terminator. The ion energy was typically 0.5 – 2.0 keV, consistently with the bulk speed of the sheath flow was 400 km/s during the period of diffuse ELF event. The number density of ions was $1\times10^{7}\ \mathrm{m}^{-3}$.

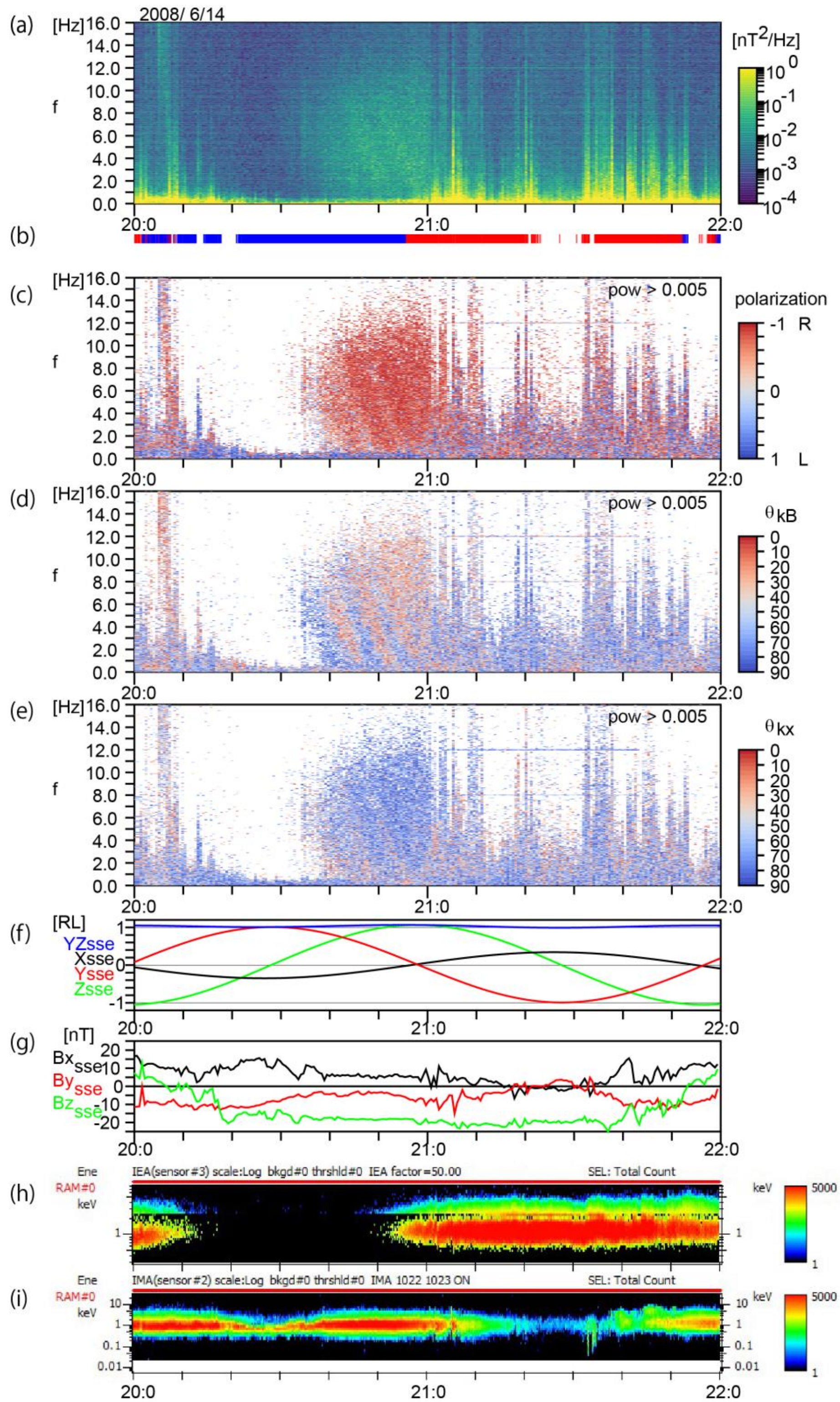

Figure 6. P A diffuse ELF event observed by Kaguya on June 14, 2008. See the legend of Figure 2.

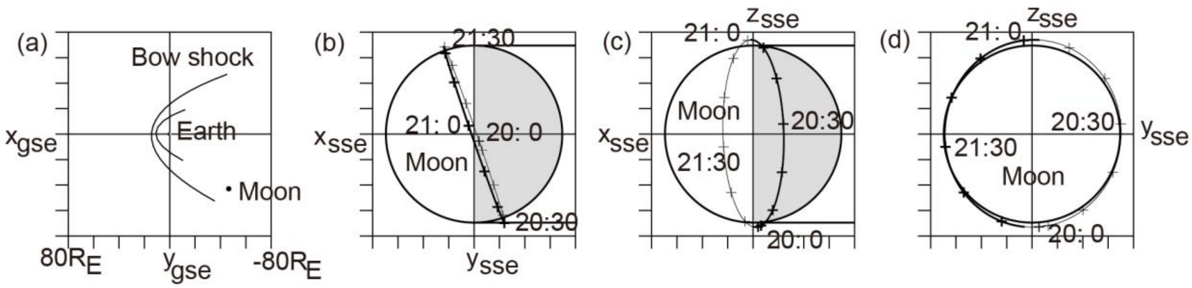

Figure 7. Position of Kaguya at the detection of the diffuse ELF waves on June 14, 2008. (a) Position of the moon in geocentric solar ecliptic (gse) coordinates. (b)(c)(d) Kaguya position projected on (b) x-y, (c) x-z, and (d) y-z planes of sse coordinate system.

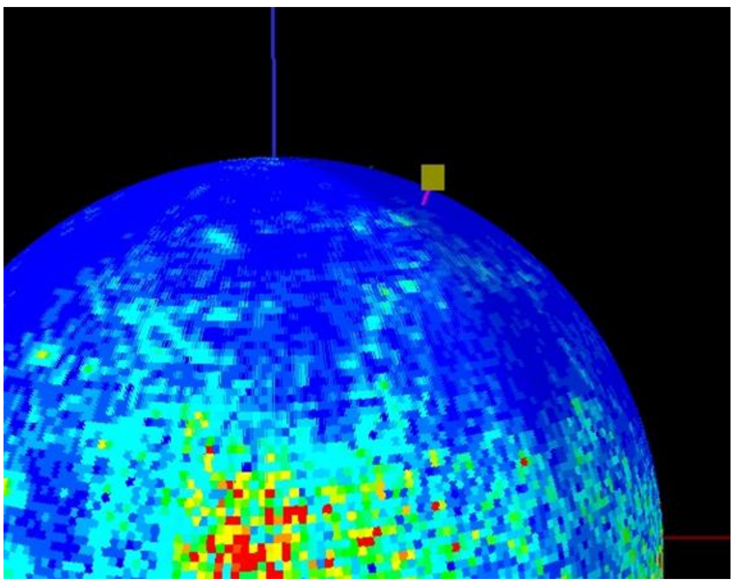

Figure 8. Magnetic connection between Kaguya (not in scale) and the lunar surface at 20:50 on June 14, 2008. The purple bar represents the direction of the magnetic field observed by Kaguya.

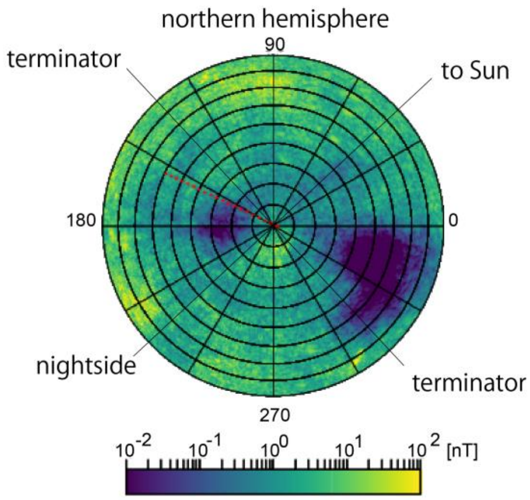

Figure 9. The position of Kaguya and the lunar crustal magnetic field on the northern hemisphere at an altitude of 0 km (Tsunakawa et al., 2015). Kaguya position from 20:40 to 20:59 were plotted every 1 minute on the Lambert azimuthal equal area projection.

4 Discussion

4.1 Summary of observation

The properties of the diffuse ELF waves observed by Kaguya around the moon are summarized as follows:

1) They are magnetic fluctuations in a frequency range from 1 to 16 Hz, between the local ion- and electron cyclotron frequencies.
2) They were right-hand polarized with respect to the background magnetic field.
3) The wave number vector was nearly parallel to the background magnetic field.
4) They were detected irrespective of magnetic connection to the lunar surface.
5) They were preferentially observed in polar region.

4.2 Possible explanation for broad frequency range

Considering the frequency range and right-handed polarization with respect to the background magnetic field, the diffuse ELF waves are thought to be whistler mode waves propagating nearly parallel to the background magnetic field. The energy source is supposed to be ions reflected by the crustal magnetic field, which have broader energy and angular distributions than the incident solar wind (Saito et al., 2010, 2012). They would form a ring-beam distribution in velocity space that can generate whistler mode waves thorough cyclotron resonance (e.g., Gary, 1991)

The broadband, diffuse emission is expected to be due to ineffectiveness of Doppler shift of the waves generated by ions reflected into directions perpendicular to the solar wind flow. If the wave number vector $\mathbf{k}$ was antiparallel to the solar wind velocity $\mathbf{V}_{sw}$, the resonant waves would be heavily Doppler-shifted and the observed bandwidth would be narrowed with reversed polarization as illustrated in Figure 10a. The dashed lines represent Doppler-shift relationship

$$\omega + \mathbf{k} \cdot \mathbf{V}_{SW} = \omega_{OBS} \qquad (1)$$

between the angular frequencies ω in the solar wind frame and ω_{OBS} in spacecraft frame. The polarization ω, positive (negative) for right-handed (left-handed) polarization, would be reversed if the $\mathbf{k} \cdot \mathbf{V}_{SW}$ term was large. In contrast, if the wave number vector $\mathbf{k}$ was perpendicular to the solar wind flow, the term $\mathbf{k} \cdot \mathbf{V}_{SW}$ would be small and would not narrow the bandwidth or reverse the polarization, as illustrated in Figure 10b.

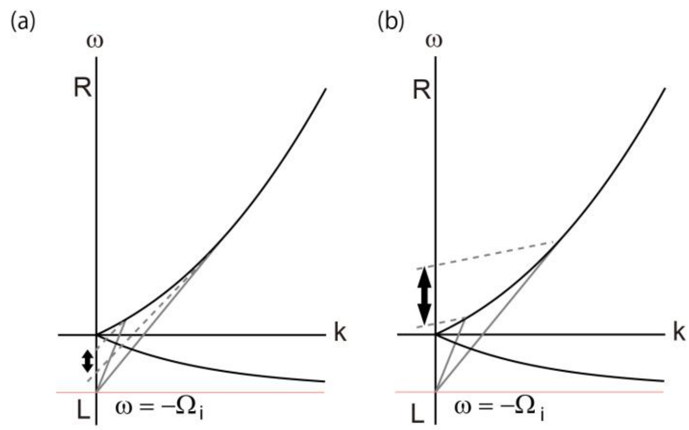

Figure 10. Schematic illustration of observed bandwidth for different Doppler-shift. Curves are dispersion diagram for plasma waves in extremely low frequency range with positive ω for right-hand polarized waves and negative ω for left-hand polarized waves, propagating parallel to the background magnetic field. Solid-lines are cyclotron resonance condition, and dashed lines represent Doppler-shift. In (a) heavy Doppler-shift case the bandwidth is narrowed and the polarization is reversed, while in (b) slight Doppler-shift case, bandwidth remains broad and polarization remains right-handed.

It turns out that the real resonance took place at higher frequency than that illustrated in Figure 10. In the following section, the resonant conditions will be investigated by using the dispersion curves drawn with parameters observed.

4.3 Dispersion relation and resonant condition

Figure 11 shows a dispersion relation $\omega(k)$ of parallel propagating whistler mode wave drawn with parameters of July 14, 2008 diffuse ELF event. The plasma density was 10 cm^{-3} and the magnitude of the magnetic field was 22.1 nT at 20:58. The observed frequency 1 – 8 Hz normalized by the ion cyclotron frequency 0.34 Hz corresponds to 3 – 24 Ω_i. The wave number vector is assumed to be parallel to the background magnetic field.

The dashed lines in Figure 11 represent Doppler-shift equation (1) for the upper and lower boundary of observed frequency. The inclination -100 km /s was calculated from the bulk flow 400 km/s observed by MAP-PACE on the assumption that the was propagating away from the moon and the $\mathbf{k}$ vector was anti-parallel to the background magnetic field (5.6, -7.6, -20.0) nT. The upper and lower lines intersect the dispersion curve at (ω, k) = (21 Ω_i, $9 \times 10^3 \Omega_i c^{-1}$) and (2 Ω_i, $3 \times 10^3 \Omega_i c^{-1}$), respectively. Thus, the frequency of the whistler mode wave in the sheath flow frame was estimated to be in the range from 0.6 Hz to 7 Hz, and the wavelength was between 100 km and 300 km.

In Figure 11, the cyclotron resonance condition of reflected ions with velocity $\mathbf{V}_R$

$$\omega + \mathbf{k}\cdot\mathbf{V}_{SW} - \mathbf{k}\cdot\mathbf{V}_R = -\Omega_i \qquad (2)$$

is represented by gray solid lines with positive inclinations. Three lines are for ions with parallel speed $V_{\parallel} \equiv (\mathbf{k}\cdot\mathbf{V}_{SW} - \mathbf{k}\cdot\mathbf{V}_R)/|\mathbf{k}|$ of 440 km/s (1 keV), 620 km/s (2 keV) and 760 km/s (3 keV) as a measure of the energy of solar wind (or magnetosheath) protons. A line with too small inclination does not intersect the curve in positive ω range. That is, too slow ions can't be resonant with the whistler mode wave. The line for 1 keV ions intersects the dispersion curve at two points around $1\,\Omega_i$ and $4\,\Omega_i$, and the latter agrees with the observed frequency range. This is different from illustrations in Figure 10 in which resonance was assumed to be at lower frequency. The lower limit of the possible intersection would be at around $2\,\Omega_i$, consistently with the lowest frequency of the detected diffuse ELF waves in the sheath flow frame.

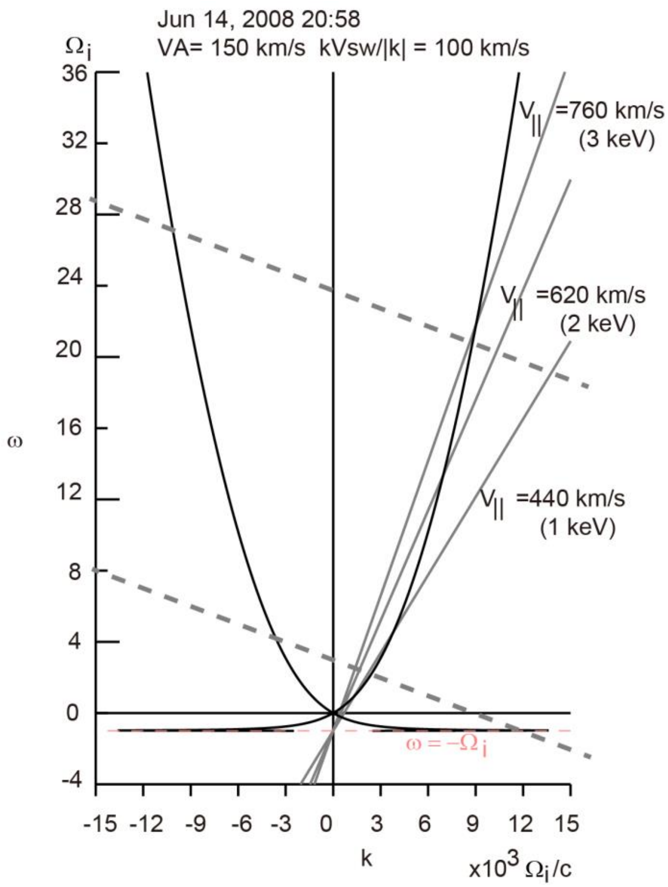

Figure 11. Dispersion diagram, cyclotron resonance condition, and Doppler-shift for the diffuse ELF waves on June 14, 2008, 20:58. The angular frequency is normalized by the magnitude of ion cyclotron frequency $|\Omega_i|$ and the wave number is normalized by $|\Omega_i|/c$, where c is the speed of light.

In order to account for the upper boundary of the observed frequency, we need $V_{\parallel} =$ 760 km/s (3 keV), about $\sqrt{3}$ times faster than the solar wind bulk speed, while we have seen the upper boundary of the ion energy was about 2 keV in the spacecraft frame of reference in Figure 6. Reflected ions with velocity $\mathbf{V}_R$ in the spacecraft frame have velocity $\mathbf{V}_R - \mathbf{V}_{sw}$ in the solar wind (or magnetosheath flow) frame of reference, but in this event, the wave number vector $\mathbf{k}$ was nearly perpendicular to the solar wind flow and the term $\mathbf{k}\cdot\mathbf{V}_{sw}$ does not contribute to $V_{\parallel}$. The reflected ions must have higher velocity than the solar wind speed to have parallel component $V_{\parallel}$ as estimated.

In Figure 6 we have seen a falling tone structure of the diffuse ELF waves. The magnetic field, plasma density and bulk velocity were stable during the period. Any distinct feature which might correspond to the falling tone structure was searched in MAP-PACE data, but no such feature was found. The decrease of frequency can be interpreted as decrease of parallel velocity component of reflected ions responsible for generation of the waves. It is not clear whether it was temporal or spatial variation. During the 5-minute interval of the 3 lanes of falling tone, Kaguya traveled about 15° in longitude. There is a possibility that the direction of velocities of reflected ions varied depending on distance from their reflection point, but it is not understood why the falling tone appeared repeatedly.

Figure 12 shows the Doppler-shift relation of the observed frequencies overlaid on a dispersion relation $\omega(k)$ of parallel propagating whistler wave for March 8, 2008 diffuse ELF event and cyclotron resonance condition. The plasma density 8 cm^{-3} and the magnitude of the magnetic field 4.9 nT at 07:05 were employed. The observed frequency 4 – 16 Hz normalized by the ion cyclotron frequency 0.075 Hz corresponds to 54 – 210 Ω_i. It should be noted that the upper boundary of the frequency range was limited by half of the sampling rate 32 Hz of the magnetic field observation.

Doppler shift was small for this case. Bulk velocity of the solar wind calculated from MAP-PACE observation was 250 km/s and the velocity component parallel to the background magnetic field (0.47, 4.6, 1.5) nT was as small as 24 km/s. The lines of Doppler-shift with positive and negative inclinations are drawn for two possible propagation directions parallel or antiparallel to the magnetic field. The frequency in the solar wind frame falls in the range from $54\pm8\Omega_i$ (4 ± 0.3 Hz) to $210\pm10\Omega_i$ (16 ± 0.75 Hz). The wave number $|\mathbf{k}|$ is estimated to be $6\times10^4|\Omega_i|/c$ – $1.2\times10^5|\Omega_i|/c$, which correspond to wavelength from 66 km to 33 km.

The gray lines in Figure 12 are cyclotron resonance conditions for ions with 3 different values of $V_{\parallel}$ = 310 km/s (0.5 keV), 440 km/s (1 keV), and 540 km/s (1.5 keV). To account for the observed frequency range, ions should have velocity components $V_{\parallel}$ in the range 310 km/s–540 km/s, that is about 1 – $\sqrt{3}$ times larger than that of the incident solar wind.

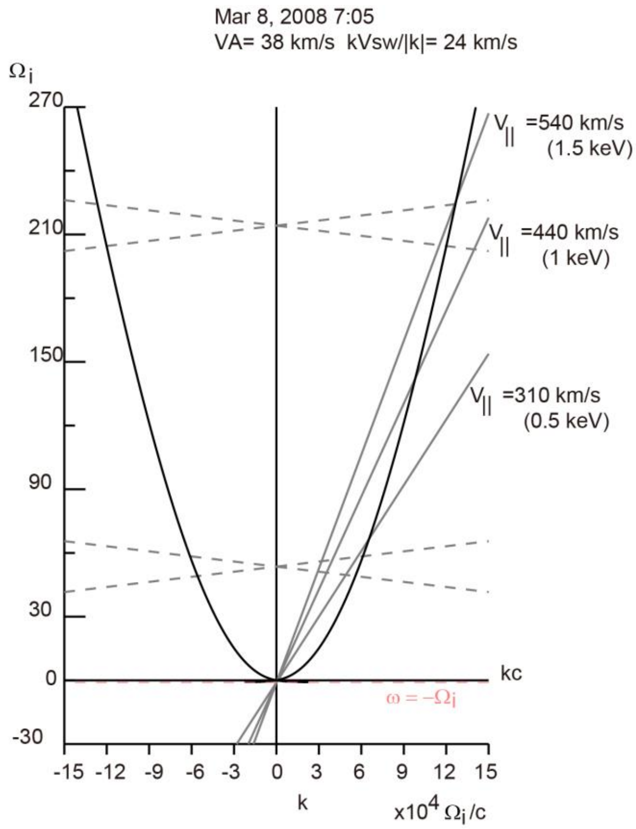

Figure 12. Dispersion diagram, cyclotron resonance condition, and Doppler-shift for the diffuse ELF waves on March 8, 2008, 7:05. See the legend of Figure 11.

4.4 Possible generation mechanism

We have seen that the velocity component $V_{\parallel}$ of reflected ions must be larger than the solar wind bulk speed to be resonant with the waves observed. On the other hand, in a magnetic field perpendicular to the solar wind flow, the velocity component $V_{\parallel}$ cannot exceed the incident speed. The speed of reflected ions can be 2 times as large as the incident speed in the solar wind frame of reference, but it contributes perpendicular component, not parallel component $V_{\parallel}$. The parallel component $V_{\parallel}$ is maximized when the ions are reflected into the direction parallel to the magnetic field with the initial speed. To obtain fast enough $V_{\parallel}$, we need initial speed larger than the solar wind bulk speed. High energy components as well as core component of solar wind ions need to be reflected into the direction of the magnetic field.

Another possibility is that the diffuse waves were generated in the upstream flow, not at Kaguya position. In Figure 2i we have seen slight disagreement in appearance/disappearance time of diffuse waves and of reflected ions. Bunches of reflected protons at around 6:55 (and 4:55) were not accompanied by diffuse ELF waves. In Figures 8 and 9 we can hardly find magnetic anomalies that would reflect incident ions. The ions responsible for the generation of diffuse waves might not be detected at Kaguya position.

Figure 13 illustrates wave generation and propagation schematically. The solar wind ions reflected by the lunar magnetic field can have large speed (Saito et al., 2010) and large gyroradius (Nishono et al., 2009, 2013). The whistler mode wave is generated in upstream solar wind by the reflected ions and begins to propagate along the magnetic field line convected by the solar wind flow. Slower components of the wave might crash into the lunar surface before they reach the limb. Only the fast-enough component of the wave can propagate to the limb (polar region or the terminator) to be detected by Kaguya. Since the group velocity of whistler mode wave is higher than the phase velocity, it can occur that the resonant ions can't reach Kaguya above the polar region. The ions might hit the moon to be absorbed by the surface or reflected by the lunar magnetic field again into different directions from that of the wave. Multiple reflection might increase the velocity of the ion by to the self-pickup process (Saito et al., 2010).

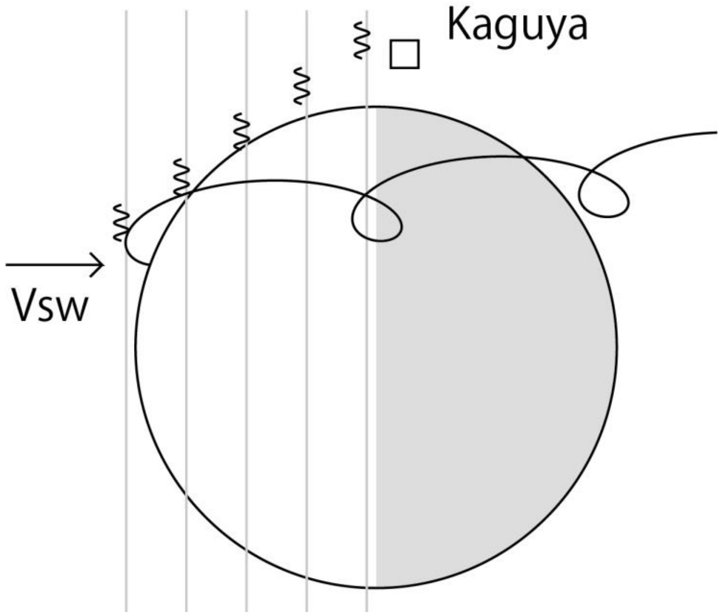

Figure 13. A schematic illustration of whistler mode wave propagating parallel to the magnetic field convected by the solar wind. The trajectory of reflected ion is not in exact direction. Position and size of Kaguya is not in scale.

5 Conclusions

Diffuse, right-hand polarized whistler mode waves propagating parallel to the magnetic field were found by Kaguya over the polar regions of the moon. They are thought to be generated by the solar wind ions reflected by the lunar magnetic field into directions perpendicular to the solar wind flow. Due to ineffectiveness of the Doppler shift, the polarization was not reversed and the frequency range was not narrowed. The reflected ions resonant with the whistler mode waves must have higher speed component parallel to the magnetic field than the solar wind bulk speed, although such higher energy ions did not necessarily accompany the diffuse waves. A possible explanation is that the cyclotron resonance occurred upstream in the solar wind above the lunar magnetic anomaly and the waves propagated along the magnetic field to the polar region during the travel time of solar wind to pass from the resonant site to the observer at the polar region.

Acknowledgments

The authors thank the Kaguya MAP-LMAG and MAP-PACE teams for the Kaguya magnetic field and plasma particle data. The Kaguya MAP-LMAG and MAP-PACE data are available at Kaguya (SELENE) Data Archive (http://l2db.selene.darts.isas.jaxa.jp/index.html.en). The authors also thank the ACE SWEPAM instrument team and the ACE Science Center for providing the ACE data. Interplanetary magnetic field parameter (MAG) and solar wind parameter (SWEPAM) data obtained by ACE are available at the ACE Science Center (http://www.srl.caltech.edu/ACE/ASC/index.html). T. Nakagawa thanks Yoshiki Sugata and Sho Ito for their contribution in event finding and examination of spatial distribution and solar wind condition. The authors declare that they have no conflicts of interests. This work was supported by JSPS KAKENHI Grant Number 18K03727.

References

Bhardwaj, A., Dhanya, M. B., Alok1, A., Barabash, S., Wieser, M., Futaana, Y., Wurz, P., Vorburger, A., Holmström, M., Lue, C., Harada, Y., & Asamura, K. (2015), A new view on the solar wind interaction with the Moon, Geosci. Lett. 2:10, DOI 10.1186/s40562-015-0027-y.

Bosqued, J. M., Lormant, N., R`eme, H., d'Uston, C., Lin, R. P., Anderson, K. A., Carlson, C. W., Ergun, R. E., Larson, D., McFadden, J., McCarthy, M. P., Parks, G. K., Sanderson, T. R., & Wenzel, K.-P. (1996), Moon solar wind interaction: First results from the WIND/3DP experiment, Geophys. Res. Lett., 23, 1259–1262, doi:10.1029/96GL00303.

Colburn, D.S., R. G. Currie, J. D. Mihalov, C. P. Sonett (1967), Diamagnetic solar-wind cavity discovered behind moon, Science, 158, 1040–1042.

Gary, S. P. (1991), Electromagnetic ion/ion instabilities and their consequences in space plasmas - A review, Space Science Reviews, 56, p. 373 – 415, doi:10.1007/BF00196632.

Halekas, J. S., Brain, D. A., Mitchell, D. L., Lin, R. P., Harrison, L. (2006a), On the occurrence of magnetic enhancements caused by solar wind interaction with lunar crustal fields. Geophys. Res. Lett. 33, L01201, doi:10.1029/2006GL025931.

Halekas, J. S., Brain, D. A., Mitchell, D. L., & Lin, R. P. (2006b), Whistler waves observed near lunar crustal magnetic sources. Geophysical Research Letters, 33, L22104. doi:10.1029/2006GL027684.

Harada, Y., Halekas, J. S., Poppe, A. R., Tsugawa, Y., Kurita, S., & McFadden, J. P. (2015), Statistical characterization of the foremoon particle and wave morphology: ARTEMIS observations. J. Geophys. Res. Space Physics, 120, 4907– 4921. doi: 10.1002/2015JA021211.

Harada, Y., & Halekas, J. S. (2016), Upstream Waves and Particles at the Moon, in *Low-Frequency Waves in Space*, chap. 18, pp. 307–322, John Wiley Sons, Inc, Hoboken, NJ, doi: 10.1002/9781119055006.

Kato, M., Sasaki, S., Takizawa, Y. & the Kaguya project team (2010), The Kaguya mission overview, *Space Sci. Rev.*, 154, 3–19, doi:10.1007/s11214-010-9678-3.

Lyon, E. F., Bridge, H. S., & Binsack, J. H. (1967), Explorer 35 plasma measurements in the vicinity of the Moon, J. Geophys. Res., 72(23), 6113– 6117, doi:10.1029/JZ072i023p06113.

Lue, C., Futaana, Y., Barabash, S., Wieser, M., Holmström, M., Bhardwaj, A., Dhanya, M. B., & Wurz, P. (2011), Strong influence of lunar crustal fields on the solar wind flow, Geophys. Res. Lett., 38, L03202, doi:10.1029/2010GL046215.

McComas, D. J., Allegrini, F., Bochsler, P., Frisch, P., Funsten, H. O., Gruntman, M., Janzen, P. H., Kucharek, H., Möbius, E., Reisenfeld, D. B., & Schwadron, N. A. (2009), Lunar backscatter and neutralization of the solar wind: First observations of neutral atoms from the Moon, Geophys. Res. Lett., 36, DOI: 10.1029/2009GL038794.

Nakagawa, T. (2016), ULF/ELF waves in the near-Moon space, in *Low-Frequency Waves in Space*, chap. 17, pp. 295–306, John Wiley Sons, Inc, Hoboken, NJ, doi:10.1002/9781119055006.

Nakagawa, T., Takahashi, F., Tsunakawa, H., Shibuya, H., Shimizu, H., & Matsushima, M. (2011). Non-monochromatic whistler waves detected by Kaguya on the dayside surface of the moon. Earth, Planets and Space, 63, 37–46, doi:10.5047/eps.2010.01.005

Nakagawa, T., Nakayama, A., Takahashi, F., Tsunakawa, H., Shibuya, H., Shimizu, H., & Matsushima, M. (2012). Large-amplitude monochromatic ULF waves detected by Kaguya at the moon. Journal of Geophysical Research, 117, A04101, doi:10.1029/2011JA017249.

Nishino, M. N., Fujimoto, M., Maezawa, K., Saito, Y., Yokota, S., Asamura, K., Tanaka, T., Tsunakawa, H., Matsushima, M., Takahashi, F., Terasawa, T., Shibuya, H., Shimizu, H. (2009) Solar-wind proton access deep into the near-Moon wake, Geophys. Res. Lett., 36, L16103, doi:10.1029/2009GL039444.

Nishino, M. N., Fujimoto, M., Saito, Y., Tsunakawa, H., Kasahara, Y., Kawamura, M., Matsushima, M., Takahashi, F., Shibuya, H., Shimizu, H., Goto, Y., Hashimoto, K., Omura, Y., Kumamoto, A., Ono, T., Yokota, S. (2013) Type-II entry of solar wind protons into the lunar wake: Effects of magnetic connection to the night-side surface, Planetary and Space Science, 87, 106-114, doi:10.1016/j.pss.2013.08.017.

Ogilvie, K. W., Steinberg, J. T., Fitzenreiter, R. J., Owen, C. J., Lazarus, A. J., Farrell, W. M., Torbert, R. B. (1996), Observation of the lunar plasma wake from the WIND spacecraft on December 27, 1994, Geophys. Res. Lett., 23, 1255-1258, doi:10.1029/96GL01069.

Poppe, A. R., Sarantos, M. Halekas, J. S., Delory, G. T., Saito, Y. Nishino, M. (2014), Anisotropic solar wind sputtering of the lunar surface induced by crustal magnetic anomalies, Geophys. Res. Lett., 41, 4865–4872, doi:10.1002/2014GL060523.

Saito, Y., S. Yokota T. Tanaka K. Asamura M. N. Nishino M. Fujimoto H. Tsunakawa H. Shibuya M. Matsushima H. Shimizu F. Takahashi T. Mukai T. Terasawa, (2008), Solar wind proton reflection at the lunar surface: Low energy ion measurement by MAP-PACE onboard SELENE (Kaguya), Geophys. Res. Lett., 35, L24205, doi:10.1029/2008GL036077.

Saito, Y., Yoshifumi Saito, Yokota, S., Asamura, K., Tanaka,T., Nishino, M. N., Yamamoto, T., Terakawa, Y., Fujimoto, M., Hasegawa, H., Hayakawa, H., Hirahara, M., Hoshino, M., Machida, S., Mukai, T., Nagai, T., Nagatsuma, T., Nakagawa, T., Nakamura, M., Oyama, K.-I., Sagawa, E., Sasaki, S., Seki, K., Shinohara, I., Terasawa, T., Tsunakawa, H., Shibuya, H., Matsushima, M., Shimizu, H., & Takahashi, F. (2010), In-flight performance and initial results of Plasma energy Angle and Composition Experiment (PACE) on SELENE (Kaguya), Space Sci. Rev., 154, 265-303, doi:10.1007/s11214-010-9647-x.

Saito, Y., Nishino, M. N., Fujimoto, M., Yamamoto, T., Yokota, S., Tsunakawa, H., Shibuya, H., Matsushima, M., Shimizu, H. & Takahashi, F. (2012), Simultaneous observation of the electron acceleration and ion deceleration over lunar magnetic anomalies, Earth Planet. Space, 64(2), 83-92, doi:10.5047/eps.2011.07.011.

Schubert, G. & Lichtenstein, B. R. (1974), Observations of moon-plasma interactions by orbital and surface experiments, Rev. Geophys. Space Phys., 12, 592-626.

Shimizu, H., Takahashi, F., Horii, N., Matsuoka, A., Matsushima, M., Shibuya, H., & Tsunakawa, H. (2008), Ground calibration of the high-sensitivity SELENE lunar magnetometer LMAG. Earth, Planets and Space, 60, 353–363, doi:10.1186/BF03352800.

Sonnerup, B. U. Ö. & Cahill, L. J. (1967), Magnetopause structure and attitude from Explorer 12 observations, J. Geophys. Res., 72(1), 171– 183, doi:10.1029/JZ072i001p00171.

Takahashi, F., Shimizu, H., Matsushima, M., Shibuya, H., Matsuoka, A., Nakazawa, S., Iijima, Y., Otake, H., & Tsunakawa, H. (2009). In-orbit calibration of the lunar magnetometer onboard SELENE (KAGUYA). Earth, Planets and Space, 61, 1269–1274.

Tsugawa, Y., Terada, N., Katoh, Ono, T., Tsunakawa, H., Takahashi, F., Shibuya, H., Shimizu, H., & Matsushima, M. (2011), Statistical analysis of monochromatic whistler waves near the Moon detected by Kaguya, Ann. Geophys., 29, 889–893, doi:10.5194/angeo-29-889-2011.

Tsugawa, Y., Katoh, Y., Terada, N., Y., Ono, T., Tsunakawa, H., Takahashi, F., Shibuya, H., Shimizu, H., Matsushima, M., Saito, Y., Yokota, S., & Nishino, M. N. (2012), Statistical study of broadband whistler-mode waves detected by Kaguya near the Moon, Geophys. Res. Lett., 39, L16101, doi:10.1029/2012GL052818.

Tsunakawa, H., Shibuya, H., Takahashi, F., Shimizu, H., Matsushima, M., Matsuoka, A., Nakazawa, S., Otake H., & Iijima Y. (2010), Lunar magnetic field observation and initial global mapping of lunar magnetic anomalies by MAP-LMAG onboard SELENE (Kaguya), Space Sci. Rev., 154, 219-251, doi:10.1007/s11214-010-9652-0.

Tsunakawa, H., F. Takahashi, H. Shimizu, H. Shibuya, and M. Matsushima (2015), Surface vector mapping of magnetic anomalies over the Moon using Kaguya and Lunar Prospector observations, J. Geophys. Res. Planets, 120, 1160–1185, doi:10.1002/2014JE004785.

Wieser, M., Barabash, S., Futaana, Y., Holmström, M., Bhardwaj, A., Sridharan, R., Dhanya, M.B., Wurz, P., Schaufelberger, A., Asamura, K. (2009), Extremely high reflection of solar wind protons as neutral hydrogen atoms from regolith in space, Planet. Space Sci., 57, 2132-2134, doi:10.1016/j.pss.2009.09.012.

Wieser, M., Barabash, S., Futaana, Y., Holmström, M., Bhardwaj, A., Sridharan, R., Dhanya, M.B., Wurz, P., Schaufelberger, A., Asamura, K. (2011), Erratum to “Extremely high reflection of solar wind protons as neutral hydrogen atoms from regolith in space”, Planet. Space Sci., 57, 798-799, doi:10.1016/j.pss.2011.01.016.